The Z_5 model of two-component dark matter

Geneviève Bélanger,[a] **Alexander Pukhov,**[b] **Carlos E. Yaguna**[c] **and Óscar Zapata**[d,e]

[a]*LAPTh, Univ. Grenoble Alpes, USMB, CNRS,*
S-74940 Annecy, France

[b]*Skobeltsyn Institute of Nuclear Physics, Moscow State University,*
Moscow 119992, Russia

[c]*Escuela de Física, Universidad Pedagógica y Tecnológica de Colombia,*
Avenida Central del Norte # 39-115, Tunja, Colombia

[d]*Instituto de Física, Universidad de Antioquia,*
Calle 70 # 52-21, Apartado Aéreo 1226, Medellín, Colombia

[e]*Abdus Salam International Centre for Theoretical Physics,*
Strada Costiera 11, 34151, Trieste, Italy

E-mail: belanger@lapth.cnrs.fr, pukhov@lapth.cnrs.fr,
carlos.yaguna@uptc.edu.co, oalberto.zapata@udea.edu.co

ABSTRACT: Scenarios for multi-component scalar dark matter based on a single Z_N ($N \geq$ 4) symmetry are simple and well-motivated. In this paper we investigate, for the first time, the phenomenology of the Z_5 model for two-component dark matter. This model, which can be seen as an extension of the well-known singlet scalar model, features two complex scalar fields — the dark matter particles — that are Standard Model singlets but have different charges under a Z_5 symmetry. The interactions allowed by the Z_5 give rise to novel processes between the dark matter particles that affect their relic densities and their detection prospects, which we study in detail. The key parameters of the model are identified and its viable regions are characterized by means of random scans. We show that, unlike the singlet scalar model, dark matter masses below the TeV are still compatible with present data. Even though the dark matter density turns out to be dominated by the lighter component, we find that current and future direct detection experiments may be sensitive to signals from both dark matter particles.

Contents

1 Introduction

Finding the correct extension of the Standard Model (SM) that accounts for the dark matter (DM) is one of the main open problems in fundamental physics today. Even if most of the models that have been proposed and studied implicitly assume that the observed dark matter density is explained by a single new particle, it does not have to be so [1–9]. Scenarios in which two or more different particles contribute to the dark matter density — multi-component dark matter models — not only are perfectly consistent with current observations but often lead to testable predictions in current and future dark matter experiments.

Among multi-component dark matter models, those featuring scalar fields that are simultaneously stabilized by a single Z_N symmetry are particularly appealing [10, 11]. For k dark matter particles, they require only k complex scalar fields that are SM singlets but have different charges under a Z_N ($N \geq 2k$). This symmetry, in turn, could be a remnant of a spontaneously broken U(1) gauge symmetry and thus be related to gauge extensions of the SM. Recently, these scenarios were systematically analyzed [12] and it was found that, surprisingly, their dark matter phenomenology has yet to be investigated in detail. With this paper, we intend to partially fill that gap.

We study the two-component dark matter model based on the Z_5 symmetry, which serves as a prototype for all the Z_N scenarios in which the dark matter particles are two *complex* scalars. Above all, we want to characterize the viable parameter space of this model and to determine its detection prospects. To that end, we first examine the dark matter relic densities, identifying the types of processes that can modify them and the key parameters they depend on. Then, the viable parameter space of the model is characterized by means of random scans, which we analyze in detail. Our results indicate that the entire range of dark matter masses is allowed, that the dark matter density is always dominated by the lighter component, and that both dark matter particles may produce signals in future direct detection experiments.

The rest of the paper is organized as follows. In the next section, our notation is introduced and the Z_5 model is briefly described — further details are relegated to the appendices. Section 3 is devoted to the dark matter phenomenology. In particular, the effect of the different parameters on the relic densities is elucidated. Our central results are obtained in section 4. In it, we first determine, via random scans, the viable parameter space of the model and then use it to predict its detection prospects. Section 5 deals with possible extensions of our work whereas section 6 presents our conclusions.

2   The model

Let us consider a scenario with two new complex scalar fields, $\phi_{1,2}$, charged under a Z_5 symmetry. The unique charge assignment (up to trivial field redefinitions) that allows both fields to be stable is [12]

$$\phi_1 \sim \omega_5, \ \ \phi_2 \sim \omega_5^2; \qquad \omega_5 = \exp(i2\pi/5). \tag{2.1}$$

These new fields — the dark matter particles — are assumed to be singlets of the SM gauge group whereas the SM particles are taken to be singlets under the Z_5. The most general Z_5-invariant scalar potential is then given by [13]

$$\mathcal{V} = \mu_H^2 |H|^2 + \lambda_H |H|^4 + \mu_1^2 |\phi_1|^2 + \lambda_{41} |\phi_1|^4 + \lambda_{S1} |H|^2 |\phi_1|^2 + \mu_2^2 |\phi_2|^2 + \lambda_{42} |\phi_2|^4 + \lambda_{S2} |H|^2 |\phi_2|^2$$
$$+ \lambda_{412} |\phi_1|^2 |\phi_2|^2 + \frac{1}{2} \left[\mu_{S1} \phi_1^2 \phi_2^* + \mu_{S2} \phi_2^2 \phi_1 + \lambda_{31} \phi_1^3 \phi_2 + \lambda_{32} \phi_1 \phi_2^{*3} + \text{H.c.} \right], \tag{2.2}$$

where H is the SM Higgs doublet. To ensure that the model describes a two-component dark matter scenario, we assume that $\phi_{1,2}$ do not acquire a vacuum expectation value and that their masses satisfy $\frac{M_1}{2} < M_2 < 2M_1$ so that both are stable. In addition, due to the symmetry of the Lagrangian, we can take, without loss of generality, ϕ_2 to be heavier than ϕ_1 and so $M_1 < M_2 < 2M_1$, which is assumed from now on. The stability conditions as well as the one-loop renormalization group equations (RGEs) for this model are given in the appendices.

Notice that the dark matter particles interact with the SM fields only through the Higgs boson. The Z_5 model is thus one example of the so-called Higgs-portal scenarios — see ref. [14] for a recent review. In addition, the dark matter particles interact among themselves through trilinear and quartic interactions. The terms in brackets in equation (2.2)

are interactions specific to the Z_5 symmetry we are considering, while the rest are present for any Z_N (see also section 5). Had we imposed a $Z_2 \times Z_2'$ instead, as often done in two-component dark matter scenarios, all the terms in brackets would be forbidden.

In total, this model contains 11 new parameters (4 dimensionful and 7 dimensionless), but two of them — λ_{41} and λ_{42} — are irrelevant for the dark matter phenomenology and can be ignored in our analysis. The parameters μ_i^2 ($i = 1, 2$), on the other hand, can be conveniently traded for the physical masses M_i of the scalar fields, so that the free parameters of the model may be taken to be M_i, λ_{Si}, λ_{412}, μ_{Si}, and λ_{3i}. The phases of $\phi_{1,2}$ can be chosen so as to make μ_{S1} and μ_{S2} real, but then λ_{31} and λ_{32} may be complex. In the following we will stick, for simplicity, to real parameters. Our goal is to study how these nine parameters affect the relic densities, shape the viable parameter space, and determine the dark matter observables.

This Z_5 model can be seen as an extension of (and shares many features with) the well-known singlet scalar model [15–17], which is based on the standard Z_2 symmetry and includes just one dark matter particle. This latter model is currently highly constrained, requiring dark matter masses right at the Higgs-resonance or above a TeV or so [18, 19]. We would like to know, therefore, whether this restriction on low dark matter masses still holds in the Z_5 model, or if the new interactions present in it weaken such bounds and allow the dark matter particles to have masses below the TeV.

3 Dark matter phenomenology

In this model, the dark matter particles and the SM particles are connected only via Higgs-portal interactions. Thus, depending on the size of the couplings λ_{Si}, both freeze-in [20, 21] and freeze-out scenarios can be envisaged for the dark matter relic densities. We will focus, in this paper, on the more compelling freeze-out realization, which has the advantage of giving rise to testable signatures in dark matter experiments.

3.1 The relic density

The full set of $2 \to 2$ processes that may contribute to the relic density in an arbitrary two-component dark matter scenario was listed in ref. [13]. They can be classified in *types* that are denoted by four digits (each a 0, 1, or 2) indicating the sector to which the particles involved in the process belong to — 0 is used for SM particles, 1 for ϕ_1 or $\phi_1^\dagger$, and 2 for ϕ_2 or $\phi_2^\dagger$. Thus, the type 2210 includes all processes with one SM particle and one ϕ_1 (or $\phi_1^\dagger$) in the final state, and with an initial state consisting of either two ϕ_2, two $\phi_2^\dagger$, or ϕ_2 and $\phi_2^\dagger$. Among the various types, the only ones not compatible with the Z_5 symmetry are 1110 and 2220. Table 1 displays all the processes that contribute to the relic densities in the Z_5 model, with their respective type.

According to the number of SM particles, these processes can be divided into three kinds: annihilation processes (two SM particles), semi-annihilation processes [22] (one SM particle), and dark matter conversion processes (no SM particles). Figures 1 and 2 display representative Feynman diagrams for semi-annihilation and dark matter conversion processes respectively. Given that some processes receive contributions from more than

ϕ_1 Processes	Type
$\phi_1 + \phi_1^\dagger \to SM + SM$	1100
$\phi_1 + \phi_1^\dagger \to \phi_2 + \phi_2^\dagger$	1122
$\phi_1^\dagger + h \to \phi_2 + \phi_2$	1022
$\phi_1 + \phi_2^\dagger \to \phi_2 + \phi_2$	1222
$\phi_1^\dagger + \phi_1^\dagger \to \phi_2 + \phi_1$	1112
$\phi_1 + \phi_2 \to \phi_2^\dagger + h$	1220
$\phi_1 + \phi_1 \to \phi_2 + h$	1120

ϕ_2 Processes	Type
$\phi_2 + \phi_2^\dagger \to SM + SM$	2200
$\phi_2 + \phi_2^\dagger \to \phi_1 + \phi_1^\dagger$	2211
$\phi_2 + \phi_2 \to \phi_1^\dagger + h$	2210
$\phi_2 + \phi_2 \to \phi_1 + \phi_2^\dagger$	2212
$\phi_2 + \phi_1 \to \phi_1^\dagger + \phi_1^\dagger$	2111
$\phi_2 + \phi_1^\dagger \to \phi_1 + h$	2110
$\phi_2 + h \to \phi_1 + \phi_1$	2011

Table 1. The $2 \to 2$ processes that are allowed in the Z_5 model and that can modify the relic density of ϕ_1 (left) and ϕ_2 (right). h denotes the SM Higgs boson. Conjugate and inverse processes are not shown.
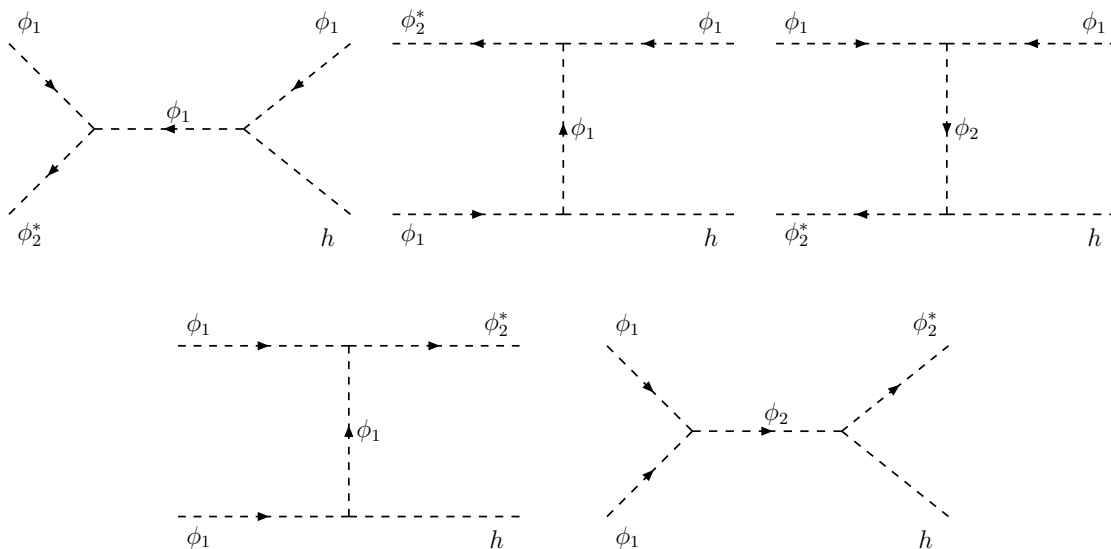

Figure 1. Dark matter semi-annihilation processes involving one trilinear μ_{S1} and one Higgs-DM λ_{Si} interactions: $\phi_1\phi_2^* \to \phi_1 h$ (top) and $\phi_2^* h \to \phi_1\phi_1$ (bottom). Replacing $\mu_{S1} \to \mu_{S2}$ similar diagrams arise for the processes $\phi_1\phi_2 \to \phi_2 h$ (top) and $\phi_2\phi_2 \to \phi_1 h$ (bottom).

one Feynman diagram, e.g. $\phi_2 + \phi_2^\dagger \to \phi_1 + \phi_1^\dagger$, interference effects are expected to play a role in certain cases. Let us also note that while the quartic couplings, λ_{3i}, induce only dark matter conversion processes, the trilinear couplings, μ_{Si}, contribute to both, semi-annihilations and conversions. The annihilations into two SM particles (not shown), on the other hand, proceed via the usual s-channel Higgs-mediated diagram, with W^+W^- being the dominant final state for $M_i \gtrsim M_W$.
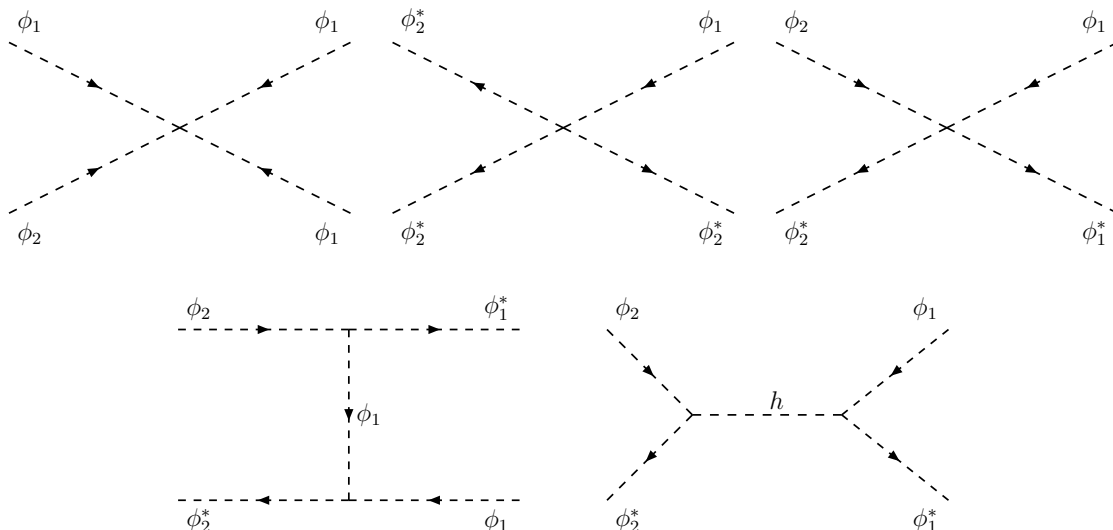
Figure 2. Dark matter conversion processes. Top: via quartic interactions — λ_{31} (left), λ_{32} (center) and λ_{412} (right). Bottom: via a μ_{S1} trilinear interaction (left) or Higgs-portal couplings (right).

The Boltzmann equations for the Z_5 model thus read

$$
\begin{aligned}
\frac{dn_1}{dt} = {}& -\sigma_v^{1100}\left(n_1^2 - \bar{n}_1^2\right) - \sigma_v^{1120}\left(n_1^2 - n_2\frac{\bar{n}_1^2}{\bar{n}_2}\right) - \sigma_v^{1122}\left(n_1^2 - n_2^2\frac{\bar{n}_1^2}{\bar{n}_2^2}\right) \\
& - \frac{1}{2}\sigma_v^{1112}\left(n_1^2 - n_1 n_2\frac{\bar{n}_1}{\bar{n}_2}\right) - \frac{1}{2}\sigma_v^{1222}\left(n_1 n_2 - n_2^2\frac{\bar{n}_1}{\bar{n}_2}\right) \\
& - \frac{1}{2}\sigma_v^{1220}\left(n_1 n_2 - n_2\bar{n}_1\right) + \frac{1}{2}\sigma_v^{2210}(n_2^2 - n_1\frac{\bar{n}_2^2}{\bar{n}_1}) - 3Hn_1\,,
\end{aligned}
\tag{3.1}
$$

$$
\begin{aligned}
\frac{dn_2}{dt} = {}& -\sigma_v^{2200}\left(n_2^2 - \bar{n}_2^2\right) - \sigma_v^{2210}\left(n_2^2 - n_1\frac{\bar{n}_2^2}{\bar{n}_1}\right) - \sigma_v^{2211}\left(n_2^2 - n_1^2\frac{\bar{n}_2^2}{\bar{n}_1^2}\right) \\
& - \frac{1}{2}\sigma_v^{2221}\left(n_2^2 - n_1 n_2\frac{\bar{n}_2}{\bar{n}_1}\right) - \frac{1}{2}\sigma_v^{1211}\left(n_1 n_2 - n_1^2\frac{\bar{n}_2}{\bar{n}_1}\right) \\
& - \frac{1}{2}\sigma_v^{1210}\left(n_1 n_2 - n_1\bar{n}_2\right) + \frac{1}{2}\sigma_v^{1120}(n_1^2 - n_2\frac{\bar{n}_1^2}{\bar{n}_2}) - 3Hn_2.
\end{aligned}
\tag{3.2}
$$

Here n_i $(i = 1, 2)$ denote the number densities of ϕ_i, and $\bar{n}_i$ their respective equilibrium values. σ_v^{abcd} stands for the thermally averaged cross section, which satisfies

$$
\bar{n}_a\bar{n}_b\sigma_v^{abcd} = \bar{n}_c\bar{n}_d\sigma_v^{cdab}.
\tag{3.3}
$$

By solving these equations, the relic densities of ϕ_1 and ϕ_2 — Ω_1 and Ω_2 — can be calculated. Since its version 4.1, `micrOMEGAs` [13] incorporated two-component dark matter scenarios, automatically including all the relevant processes for a given model and numerically solving the corresponding Boltzmann equations. It also includes the code files of the Z_5 model we are studying. We will rely on `micrOMEGAs` [13, 23, 24] to compute the relic densities and the dark matter detection observables. Keep in mind, though, that in the

course of this work we found and corrected some bugs affecting the calculation of the relic density for two dark matter particles. To reproduce our results, `microMEGAs` version 5.2 or later should be used.

To estimate the relevance of the three kinds of processes — annihilations, semi-annihilations, and conversions — that can contribute to the relic density of ϕ_1, it is convenient to define the following three parameters

$$\zeta_{\text{anni}}^1 \equiv \frac{\sigma_v^{1100}}{\overline{\sigma_v^1}}, \quad \zeta_{\text{semi}}^1 \equiv \frac{\frac{1}{2}(\sigma_v^{1120} + \sigma_v^{1220} + \sigma_v^{1022})}{\overline{\sigma_v^1}}, \quad \zeta_{\text{conv}}^1 \equiv \frac{\sigma_v^{1122} + \sigma_v^{1112} + \sigma_v^{1222}}{\overline{\sigma_v^1}}, \quad (3.4)$$

with

$$\overline{\sigma_v^1} \equiv \sigma_v^{1100} + \frac{1}{2}\sigma_v^{1120} + \sigma_v^{1122} + \sigma_v^{1112} + \sigma_v^{1222} + \frac{1}{2}\sigma_v^{1220} + \frac{1}{2}\sigma_v^{1022}. \quad (3.5)$$

These parameters are assumed to be evaluated at a temperature typical of the freeze-out process — $M_1/25$ for definiteness. Each of them varies between 0 and 1 depending on how important the respective type of process is. Thus, $\zeta_{\text{semi}}^1 \approx 1$ indicates that the ϕ_1 relic density is mostly driven by semi-annihilations. Notice that they are normalized such that $\zeta_{\text{anni}}^1 + \zeta_{\text{semi}}^1 + \zeta_{\text{conv}}^1 = 1$. Analogous parameters can be defined for ϕ_2. If a more detailed pictured is required of how the different processes affect the relic density, `microMEGAs` has the option, since its version 5.2, to exclude from the calculation one or more types of processes via the variable `Excludefor2DM`. We have used this option to perform several checks on our results.

Semi-annihilation processes will play a crucial role in our analysis so it is useful to get a feeling of how they compare against the usual annihilation processes. When ϕ_1 annihilations are mediated by the typical Higgs portal, the thermally averaged cross section goes as

$$\sigma_v^{1100} \sim \frac{\lambda_{S_1}^2}{16\pi M_1^2} \qquad \text{for } M_1 \gg m_h. \quad (3.6)$$

The semi-annihilation processes $\phi_1 + \phi_1 \to h + \phi_2$, on the other hand, feature a thermally averaged cross section

$$\sigma_v^{1120} \sim \frac{\mu_{S1}^2 v_H^2 \lambda_{S1}^2}{16\pi M_1^6} \qquad \text{for } \lambda_{S2} \ll \lambda_{S1}, \ M_1 \ll m_h. \quad (3.7)$$

Since σ_v^{1120} rapidly decreases with M_1, semi-annihilations are expected to stop being efficient at high values of M_1.

In the following section, we will impose the relic density constraint,

$$\Omega_1 + \Omega_2 = \Omega_{\text{DM}}, \quad (3.8)$$

where Ω_{DM} is the observed value of the dark matter density. The fraction of the total dark matter density that is accounted for by each dark matter particle is then given by the parameters

$$\xi_i = \frac{\Omega_i}{\Omega_{\text{DM}}} \quad (i = 1, 2), \quad (3.9)$$

with $\xi_1 + \xi_2 = 1$. One of the main questions in two-component dark matter scenarios is determining what these fractions are (can they be comparable?), and they also affect the dark matter detection signals, as shown next.

3.2 Direct and indirect detection

The elastic scattering of the dark matter particles off nuclei are possible thanks to the Higgs portal interaction λ_{Si}, just as in the singlet scalar model [15–17]. The expression for the spin-independent (SI) cross-section reads

$$\sigma_i^{\text{SI}} = \frac{\lambda_{Si}^2}{4\pi} \frac{\mu_R^2 m_p^2 f_p^2}{m_h^4 M_i^2}. \tag{3.10}$$

where μ_R is the reduced mass, m_p the proton mass and $f_p \approx 0.3$ is the quark content of the proton. But since we have two dark matter particles, the quantity to be compared against the direct detection limits provided by the experimental collaborations is not the cross section itself but rather the product $\xi_i \sigma_i^{\text{SI}}$.

Such direct detection limits usually provide very strong constraints on Higgs-portal scenarios like the Z_5 model we are discussing. For example, in the limit $\Omega_2 \ll \Omega_1$ and with the new Z_5 interactions switched off — where the singlet complex scalar DM model [15–17] is recovered — we get that

$$\lambda_{S1} \sim 0.3 \left(\frac{M_1}{1\,\text{TeV}} \right) \qquad \text{for } m_h \ll M_1, \tag{3.11}$$

in order to fulfill $\Omega_1 = \Omega_{\text{DM}}$. Taking into account the upper limit set by the XENON1T collaboration [25] it follows that $M_1 \gtrsim 2\,\text{TeV}$ (for a real scalar the lower limit is $\sim 950\,\text{GeV}$). Hence, for $M_1 \lesssim 2\,\text{TeV}$ the Z_5-invariant interactions must be required in order to simultaneously satisfy the relic density constraint and current direct detection limits — a result we will numerically confirm in the next section. In our analysis, we will consider the current direct detection limit set by the XENON1T collaboration [25] as well as the projected sensitivities of LZ [26] and DARWIN [27].

Regarding indirect detection, the relevant particle physics quantity switches from $\langle \sigma v \rangle$ to $\xi_i \xi_j \langle \sigma v \rangle_{ij}$, where $\langle \sigma v \rangle_{ij}$ is the cross section times velocity for the annihilation process of dark matter particles i and j into a certain final state. The main novelty in our model is the possible appearance of semi-annihilation processes involving two different dark matter particles, such as $\phi_1 + \phi_1 \rightarrow \phi_2 + h$ or $\phi_1 + \phi_2^\dagger \rightarrow \phi_1^\dagger + h$. We will rely on the indirect detection limits and on the projected sensitivities reported by the Fermi collaboration from observations of dShps [28, 29].

3.3 Parameter dependence

To study how the different parameters affect the relic densities of the dark matter particles, we first define a *reference* model in which most of these parameters are set to zero, and then switch them on, one by one, while comparing the resulting relic densities against the predictions of the reference model. The non-zero parameters of the reference model are just four: the dark matter masses (M_1, M_2) and the Higgs-portal couplings $(\lambda_{S1}, \lambda_{S2})$.
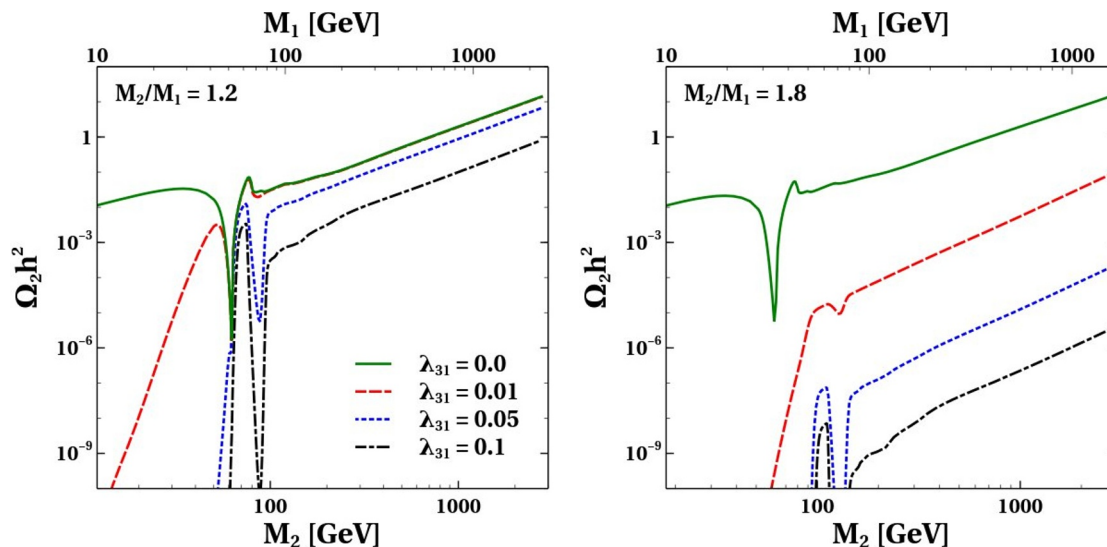
Figure 3. The effect of λ_{31} on Ω_2 for two different values of M_2/M_1: 1.2 (left panel) and 1.8 (right panel).

Note that even in this very simplified framework the relic densities are coupled via the Higgs-mediated processes $\phi_2 + \phi_2^\dagger \leftrightarrow \phi_1 + \phi_1^\dagger$ (see bottom-right panel in figure 2).

For definiteness, in this section we set $\lambda_{S1} = \lambda_{S2} = 0.1$, and examine two different values for the ratio M_2/M_1 (which can vary between 1 and 2): 1.2 and 1.8. In the following figures, the predictions of the reference model are shown in solid (green) lines. First, we are going to investigate the dependence of the relic densities on the dimensionless couplings $(\lambda_{31}, \lambda_{32}, \lambda_{412})$ and then we move on to the dimensionful ones — μ_{S1} and μ_{S2}.

3.3.1 The effect of λ's

The dimensionless couplings — $\lambda_{31}, \lambda_{32}, \lambda_{412}$ — induce the dark matter conversion processes shown in the top row of figure 2. Neither semi-annihilations nor annihilations can be caused by these couplings. λ_{31}, for instance, leads to the conversion processes $\phi_1 + \phi_2 \leftrightarrow \phi_1^\dagger + \phi_1^\dagger$ and their complex conjugates. During the ϕ_2 freeze-out, they contribute to the depletion of ϕ_2 and should therefore reduce Ω_2. Ω_1, on the other hand, should hardly get modified unless $M_1 \approx M_2$, when the kinematic suppression of $\phi_1 + \phi_1 \rightarrow \phi_1^\dagger + \phi_2^\dagger$ is alleviated. Figure 3 shows Ω_2 as a function of M_2 for $M_2/M_1 = 1.2$ (left panel), 1.8 (right panel) and for different values of λ_{31}: 0.0 (solid line), 0.01 (dashed line), 0.05 (dotted line), and 0.1 (dash-dotted line). As expected, Ω_2 decreases with λ_{31} for both values of M_2/M_1. What is a bit surprising is the size of the effect. Notice, in fact, that even a value of λ_{31} as small as 10^{-2} can modify Ω_2 by several orders of magnitude. The reason behind this behavior is that the Boltzmann equation has a term of the form ($Y_i = n_i/s$)

$$\frac{dY_2}{dT} \propto \frac{1}{2}\sigma_v^{1211} Y_1 Y_2 \qquad (3.12)$$

which exponentially suppresses the ϕ_2 density over a range of temperatures. Thus, even a moderate value of σ_v^{1211} can have a large impact on Ω_2. And the larger M_2/M_1, the
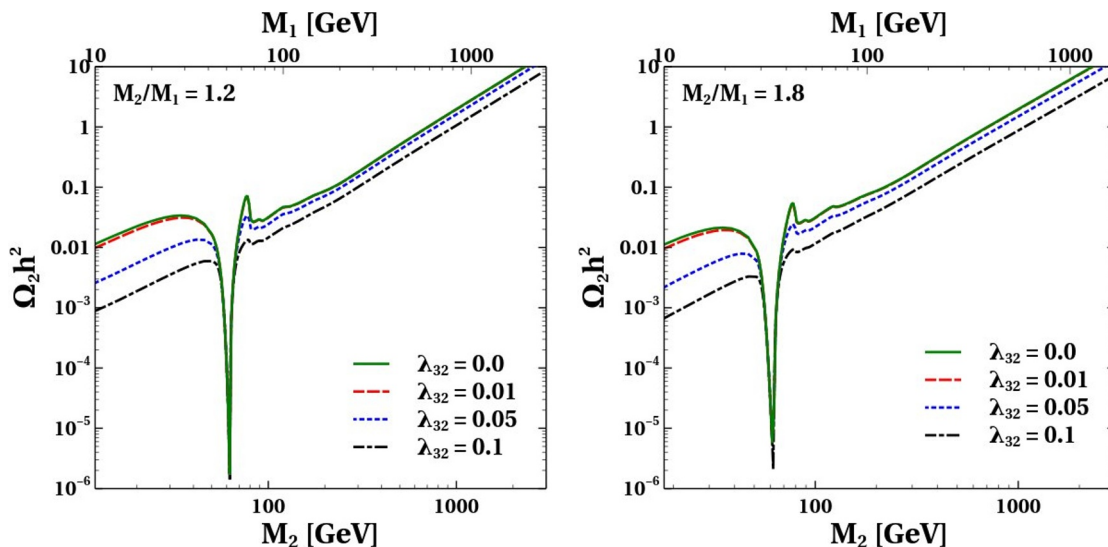
– 8 –

Figure 4. The effect of λ_{32} on Ω_2 for two different values of M_2/M_1: 1.2 (left panel) and 1.8 (right panel).

larger the suppression is. The other prominent feature in this figure is the dip observed above the Higgs resonance. It is actually caused by the usual bump in the ϕ_1 relic density for $M_h/2 \lesssim M_1 \lesssim M_W$. Because the two relic densities are coupled, the increase in Y_1 provokes a reduction in Y_2. Notice, from the top axis, that the dip indeed occurs at the expected value of M_1.

Figure 4 displays the effect on Ω_2 of λ_{32}. This coupling causes the conversion processes $\phi_2 + \phi_2 \leftrightarrow \phi_1 + \phi_2^\dagger$, which should lead to a reduction of Ω_2 while leaving Ω_1 mostly unaffected — since $\phi_1 + \phi_2^\dagger \to \phi_2 + \phi_2$ is kinematically suppressed during ϕ_1 freeze-out for $M_2 > M_1$. From the figure, we see that Ω_2 indeed decreases with λ_{32} and that the effect is pretty much independent on M_2/M_1 — the two panels seem identical (they are not). For the values of λ_{32} shown, the reduction in Ω_2 reaches at most one order of magnitude.

The last quartic coupling to be examined is λ_{412}, which should naively cause a reduction of Ω_2 via the process $\phi_2 + \phi_2^\dagger \to \phi_1 + \phi_1^\dagger$. Unlike the previous processes, however, this one receives an additional contribution from a Higgs-mediated diagram, and so interference effects between the two diagrams may play role and result in either an increase or a decrease of the relic density. The Higgs-mediated amplitude is proportional to $\lambda_{S1}\lambda_{S2}$ and its sign changes (due to the propagator) at the Higgs resonance, $M_2 \sim M_h/2$. Thus, the sign of λ_{412} turns out to be relevant in the analysis. To illustrate these effects, figure 5 shows the relic density for $M_2/M_1 = 1.2$ and different values of λ_{412} — they are positive in the left panel and negative in the right panel. From the figure the interference effects are evident. If $|\lambda_{412}| = 0.05$, for instance, Ω_2 is larger below the resonance and (sligthly) smaller above the resonance for a positive coupling (see left panel), but the other way around for a negative coupling (see right panel). On the other hand, if λ_{412} is large enough, say 0.5 (dash-dotted line), the interference effect is not as important (except very near the Higgs resonance) and the net result is that Ω_2 decreases regardless of the sign of λ_{412}. For the
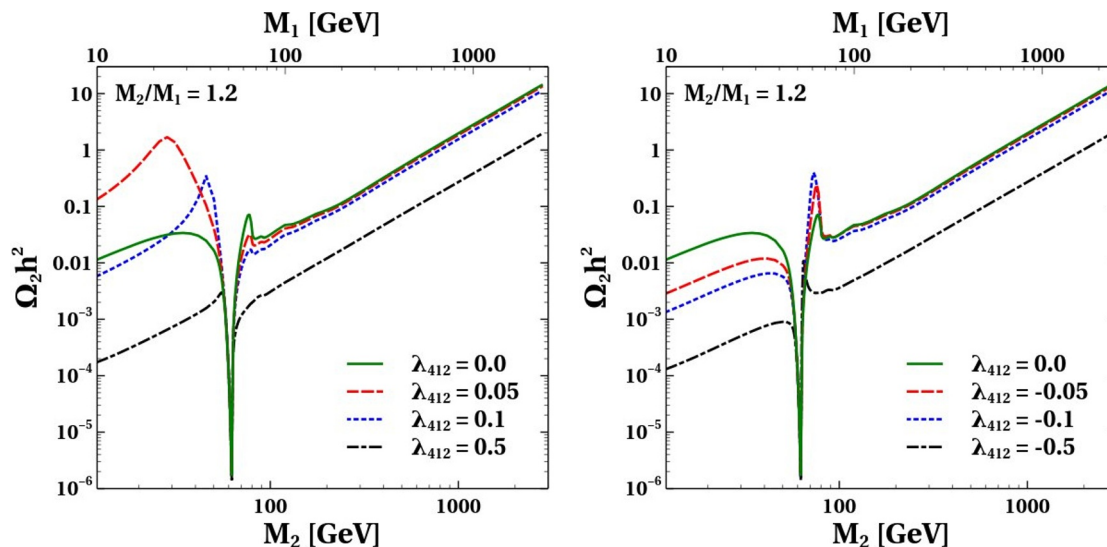
Figure 5. The effect of λ_{412} on Ω_2 for $M_2/M_1 = 1.2$. The difference between the left and the right panel is just the sign of λ_{412}.

couplings considered in figure 5, the maximum variation in Ω_2 amounts to two orders of magnitude for masses below the Higgs resonance, and one order of magnitude above it. For $M_2/M_1 = 1.8$, the results are essentially identical, so they are not shown.

As we have seen, a common feature of the quartic interactions is that they *mostly* affect the relic density of the heavier dark matter particle, Ω_2. For the parameter values we have considered in this section, the effect on Ω_1 is negligible. Thus, the ϕ_1 relic density is determined by the characteristic Higgs-mediated interactions of the singlet scalar model, and it is therefore expected to be subject to the same stringent direct detection constraints as that model. The trilinear couplings, μ_{S1} and μ_{S2}, might influence Ω_1 and help relax such constraints.

3.3.2 The effect of μ's

The trilinear couplings, μ_{S1} and μ_{S2}, give rise to both semi-annihilation and conversion processes — see figures 1 and 2. The semi-annihilation processes involve also one Higgs-dark matter coupling, either λ_{S1} or λ_{S2}, and always feature a Higgs boson as an external particle. The conversion processes, on the other hand, depend only on μ_{Si} and are mediated by a dark matter particle in the t-channel. To illustrate how these processes alter the dark matter relic densities, in this section we consider three possible values for μ_{Si}: $0.3, 1, 3$ TeV.

μ_{S1} induces the processes $\phi_1 + \phi_2^\dagger \leftrightarrow \phi_1 + h$ and $\phi_1 + \phi_1 \leftrightarrow \phi_2^\dagger + h$, the former affect only Ω_2 while the latter may affect both relic densities. Figure 6 displays Ω_i versus M_i for different values of μ_{S1} and for $M_2/M_1 = 1.2$. From the left panel we see that Ω_2 can be suppressed by orders of magnitude as a consequence of the exponential behaviour mentioned previously but now involving σ_v^{1210}. Notice also that Ω_2 increases steeply as soon as the process $\phi_1 + \phi_1 \rightarrow \phi_2 + h$ is kinematically open, as observed in the figure. From the right panel, we notice instead that, at intermediate values of M_1, Ω_1 can be
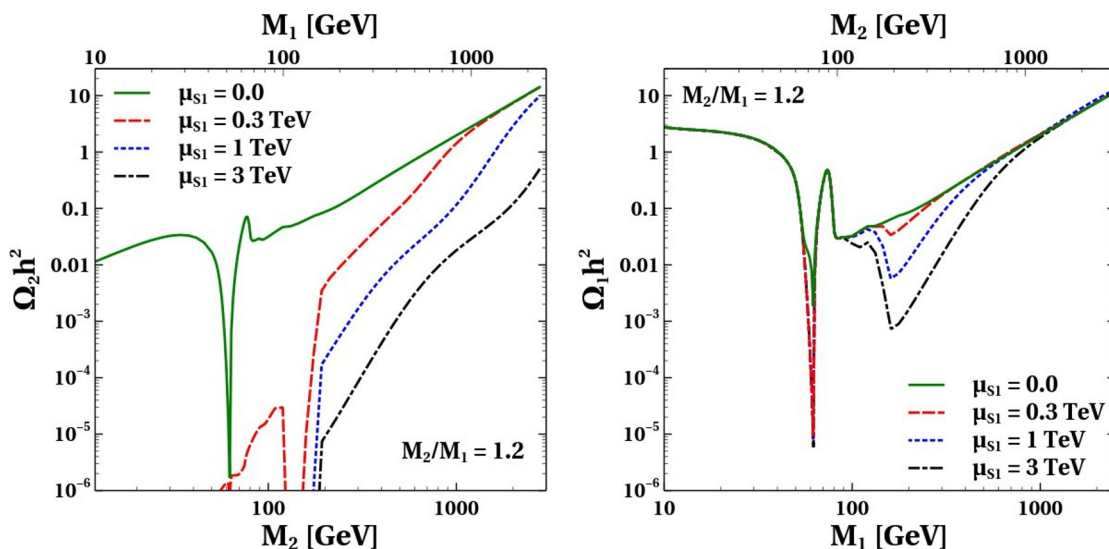
Figure 6. The effect of μ_{S1} on Ω_2 (left panel) and Ω_1 (right panel) for $M_2/M_1 = 1.2$.
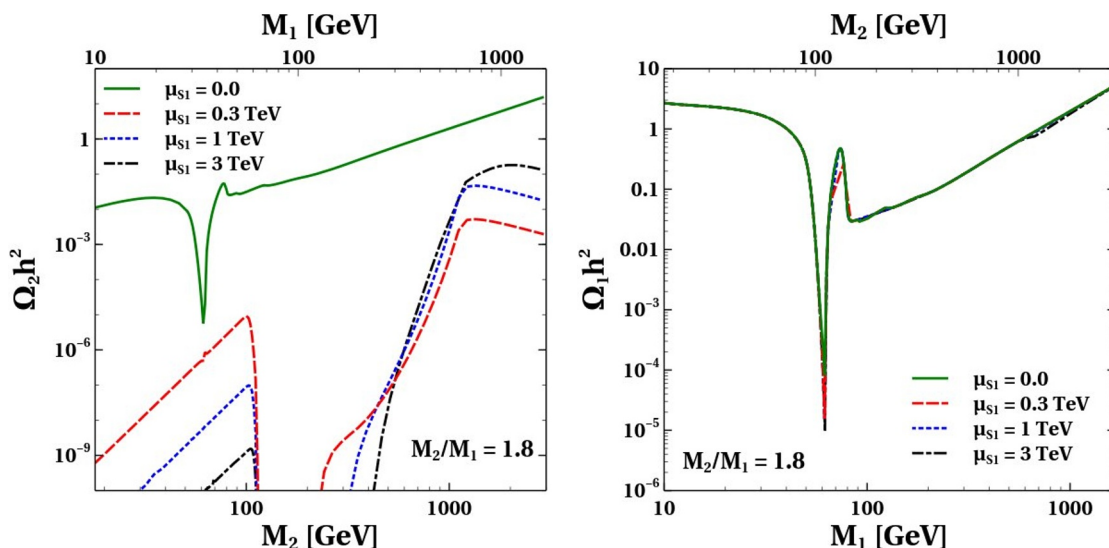

Figure 7. The effect of μ_{S1} on Ω_2 (left panel) and Ω_1 (right panel) for $M_2/M_1 = 1.8$.

reduced by up to two orders of magnitude. At low masses, the process $\phi_1 + \phi_1 \to \phi_2^\dagger + h$ is kinematically closed during ϕ_1 freeze-out, so there is no effect on Ω_1, in agreement with the figure. At high masses, it is instead the propagator that suppresses the $\phi_1 + \phi_1 \to \phi_2^\dagger + h$ diagram with respect to the standard Higgs-mediated processes. That is why there exists a finite range at moderate values of M_1 within which μ_{S1} can induce a reduction in Ω_1 — see equation (3.7). For $M_2/M_1 = 1.8$ (figure 7) the impact on Ω_1 becomes negligible while Ω_2 is even more suppressed.

Regarding the μ_{S2}-induced processes, they can affect Ω_2 at low and intermediate masses as shown in figure 8. The only process that may reduce the ϕ_1 number density after ϕ_2 freeze-out is $\phi_1 + \phi_2 \to \phi_2 + h$ but it has a negligible effect on Ω_1 due to the small value of Ω_2.
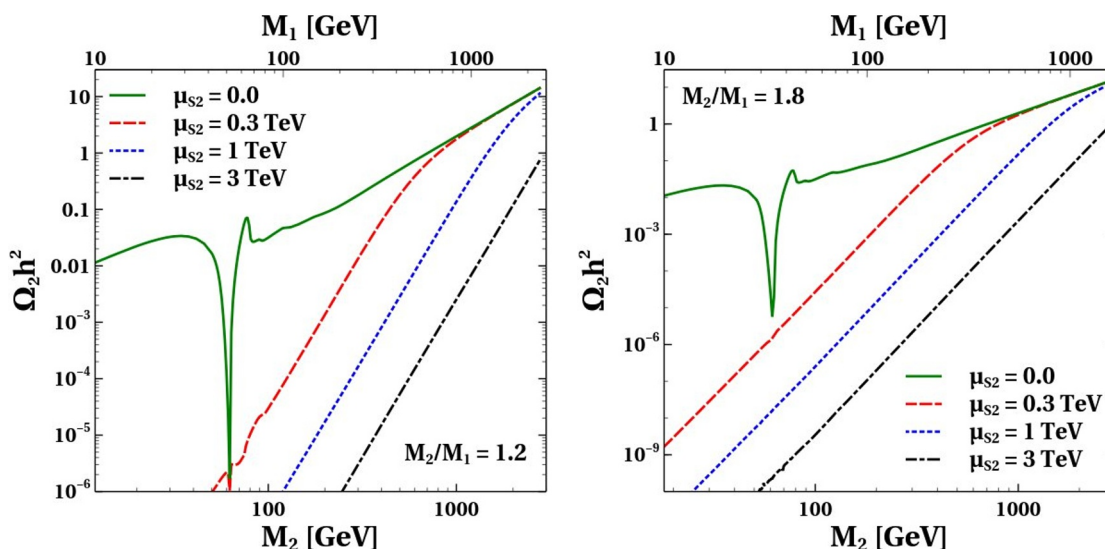
Figure 8. The effect of μ_{S2} on Ω_2 for $M_2/M_1 = 1.2$ (left panel) and $M_2/M_1 = 1.8$ (right panel). There is no appreciable effect on Ω_1 for the values considered in this figure.

4   The viable parameter space

As we have seen, both relic densities may be modified by the new interactions allowed by the Z_5 symmetry. Now we want to explore in detail their implications on the viable parameter space of this model and on the dark matter detection prospects. To that end, we have randomly scanned the parameter space of the model and selected a large sample of points consistent with current data. In particular, they are compatible with the limit on the invisible decays of the Higgs boson obtained from the LHC data [30],[1] with the direct detection limits recently derived by the XENON1T collaboration [25] (we apply the corresponding recasted exclusion given by `micrOMEGAs` [32]) and with the dark matter density as measured by PLANCK [33]. While the PLANCK collaboration reports

$$\Omega_{\mathrm{DM}} h^2 = 0.1198 \pm 0.0012, \tag{4.1}$$

the theoretical prediction of the relic density is not expected to be that precise. In our scans, we consider a model compatible with the above value if its relic density, as given by `micrOMEGAs`, lies between 0.11 and 0.13, which amounts to about a 10% uncertainty. In any case, our results are robust against plausible variations in such interval.

We have performed several random scans, varying just a subset of the free parameters of the model at a time so as to make the analysis simpler. In all the scans, the dark matter

---

[1]Very recently this result has been updated (from $\mathcal{B}_{inv} < 0.15$ to 0.13) [31] but this will not have an impact on our results.

masses and the Higgs-portal couplings are varied in the following ranges:

$$40\,\text{GeV} \leq M_1 \leq 2\,\text{TeV}, \tag{4.2}$$

$$M_1 < M_2 < 2M_1, \tag{4.3}$$

$$10^{-4} \leq |\lambda_{S1}| \leq 1, \tag{4.4}$$

$$10^{-3} \leq |\lambda_{S2}| \leq 1. \tag{4.5}$$

If these were the only parameters different from zero, the viable points would all lie at the Higgs resonance. The interplay between the relic density constraint and the strong limits from direct detection searches would exclude the rest of the parameter space. And this conclusion still holds after allowing λ_{412} to be different from zero. Thus, it is up to the new Z_5 trilinear and quartic couplings to render this model viable over most of the dark matter mass range.

To bypass the direct detection bounds, the relic density of ϕ_1 must be reduced by the new interactions. In the previous section, we saw that the parameter μ_{S1} can have this effect, so in our first scan we set the dimensionless couplings as well as μ_{S2} to zero $(\lambda_{3i}, \lambda_{412} = 0, \mu_{S2} = 0)$ and vary μ_{S1} between $0.1\,\text{TeV}$ and $10\,\text{TeV}$. This upper limit on μ_{S1} is rather arbitrary but seems reasonable given that M_1 and M_2 — the other dimensionful parameters of the model — take a maximum value of $2\,\text{TeV}$ and $4\,\text{TeV}$ respectively.

The resulting viable parameter space is shown in figure 9. Notice that the viable points cover the entire spectrum of dark matter masses, from the Higgs resonance up to the maximum value considered in the scan. This is one of our main results. From the top-left panel, we see that the ratio M_2/M_1 varies over a wide range, indicating that the dark matter particles do not need to be degenerate. In these plots, the relevance of semi-annihilation processes is color-coded in terms of ζ_{semi}^1 — see equation (3.4). Semi-annihilations are essential in the intermediate mass region $(200 < M_1/\text{GeV} < 1000)$, with most points featuring $\zeta_{\text{semi}}^1 > 0.75$. At low masses $(M_1 \lesssim 200\,\text{GeV})$, semi-annihilations are kinematically suppressed whereas at high masses $(M_1 \gtrsim 1.5\,\text{TeV})$ they are required but not as efficient. In fact, the minimum value of μ_{S1} increases with M_1 up to about $1\,\text{TeV}$ (top-right panel), when it reaches the maximum value allowed in the scan $(10\,\text{TeV})$. Had we considered higher values of μ_{S1}, semi-annihilations would have remained significant to larger dark matter masses. The Higgs-portal couplings are shown in the bottom panels. $|\lambda_{S1}|$ can vary over orders of magnitude while semi-annihilations are relevant, $M_1 < 1\,\text{TeV}$, but from then on annihilations become important and $|\lambda_{S1}|$ is therefore restricted to a narrow band, reaching 1 for $M_1 \sim 2\,\text{TeV}$. The distribution of $|\lambda_{S2}|$ tends to be concentrated toward higher values (see bottom-left panel), with a significant fraction of models featuring $|\lambda_{S2}| \geq 0.1$ for $M_1 < 1\,\text{TeV}$ $(M_2 < 2\,\text{TeV})$. As we will see, this result has important implications for the dark matter detection prospects in this model.

We already learned, from figure 9, that semi-anninilations are important in the intermediate mass region. But what about conversions and annihilations? The left panel of figure 10 shows the viable models in the plane $(\zeta_{\text{semi}}^1, \zeta_{\text{anni}}^1)$ — see equation (3.4) — with the color indicating the value of M_1. The value of ζ_{conv}^1 can be deduced from the figure by noting that $\zeta_{\text{semi}}^1 + \zeta_{\text{anni}}^1 + \zeta_{\text{conv}}^1 = 1$. By definition, all models have to lie either inside the
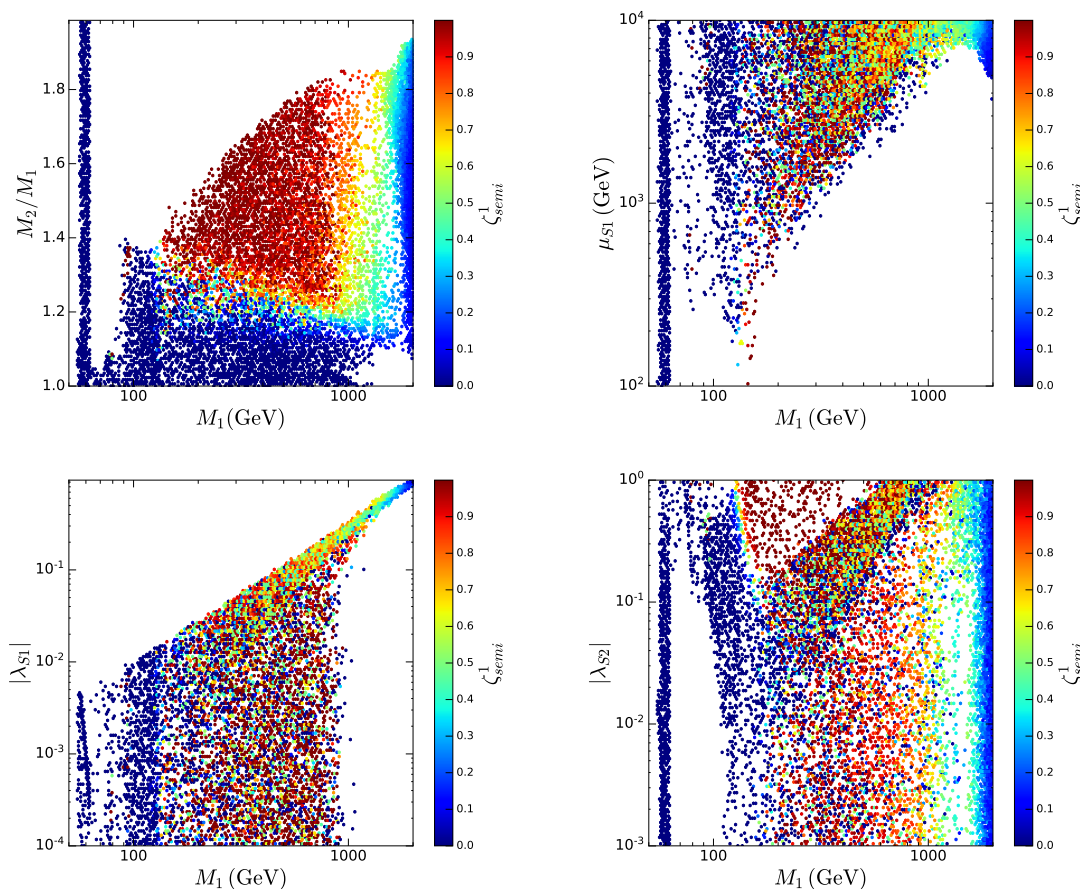
Figure 9. Viable parameter space for $\mu_{S2} = 0$ and $\lambda_{3i} = \lambda_{412} = 0$. The free parameters $(M_2/M_1, \mu_{S2}, |\lambda_{Si}|)$ are displayed as a function of ϕ_1 mass and characterized by the semi-annihilation fraction ζ^1_{semi}.

triangle with vertices $(0,0)$, $(1,0)$ and $(0,1)$, when all three types of processes contribute to the relic density; or along its edges, when the contribution from one type is negligible. This latter case is seen to be the most common, with the negligible type depending on M_1: semi-annihilations at low masses, annihilations at intermediate values, and conversions at high masses.

Regarding the contributions of the two dark matter particles to the total density, we see, from the right panel of figure 10, that ϕ_1 always gives the dominant contribution. It accounts for more than 70% of the dark matter density and in most points for more than 95% of it. In numerous cases Ω_2 turns out to be several orders of magnitude smaller than Ω_1. This hierarchy can be understood as a consequence of the fact that the new Z_5 interactions couple both dark matter particles and, as we saw in the previous section, they suppress the relic density of the heavier particle more than that of the lighter one (since the heavier can annihilate into the lighter). The fact that the lighter dark matter particle usually accounts for the bulk of the dark matter density is one of our most important results.
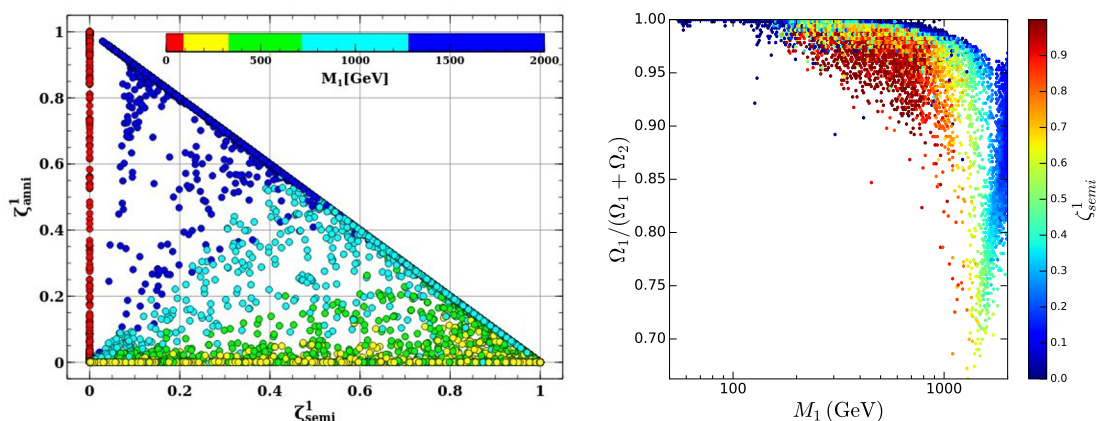
Figure 10. Semi-annihilation and annihilation fractions (left panel) and the relative contribution of ϕ_1 to the total DM relic abundance as a function of M_1 (right panel) for the scan with $0.1 \leq \mu_{S1} \leq 10\,\mathrm{TeV}$, $\mu_{S2} = 0$ and $\lambda_{3i} = \lambda_{412} = 0$.
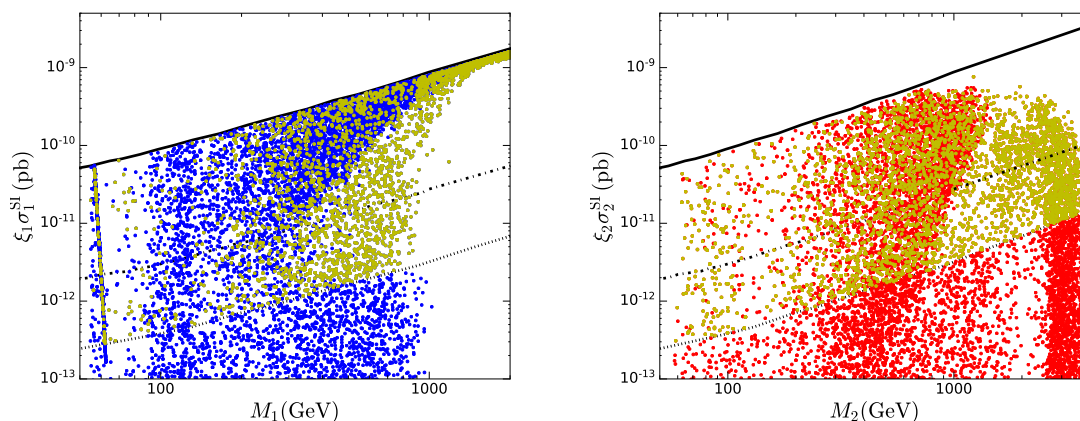

Figure 11. Spin-independent cross-sections for elastic scattering of ϕ_i with nuclei scaled by ξ_i in the scan with $\mu_{S1} \neq 0$. The solid line is the upper limit set by XENON1T collaboration [25] while the dot-dashed and dotted lines show the projected sensitivity of LZ [26] and DARWIN [27] experiments. Yellow points indicate that both DM particles lay within the sensitivity region of DARWIN.

At first sight, this distribution of the dark matter densities may seem to imply that the Z_5 model *effectively* becomes, at present, a one-component dark matter model — that ϕ_2, having a small density, can be ignored. But this is not so. From figure 11 we see that either dark matter particle may be observed in future direct detection experiments. The solid line shows the current limit from XENON1T while the dashed and dotted lines correspond to the expected sensitivities of LZ [26] and DARWIN [27] respectively. What is happening with ϕ_2 is that its smaller density can be compensated by its larger coupling to the Higgs (see figure 9), resulting in a sizable signal. The feasibility of detecting a subdominant component of the dark matter has been noted before [34, 35], but it seems to have been largely forgotten. In the Z_5 model, this possibility arises naturally.
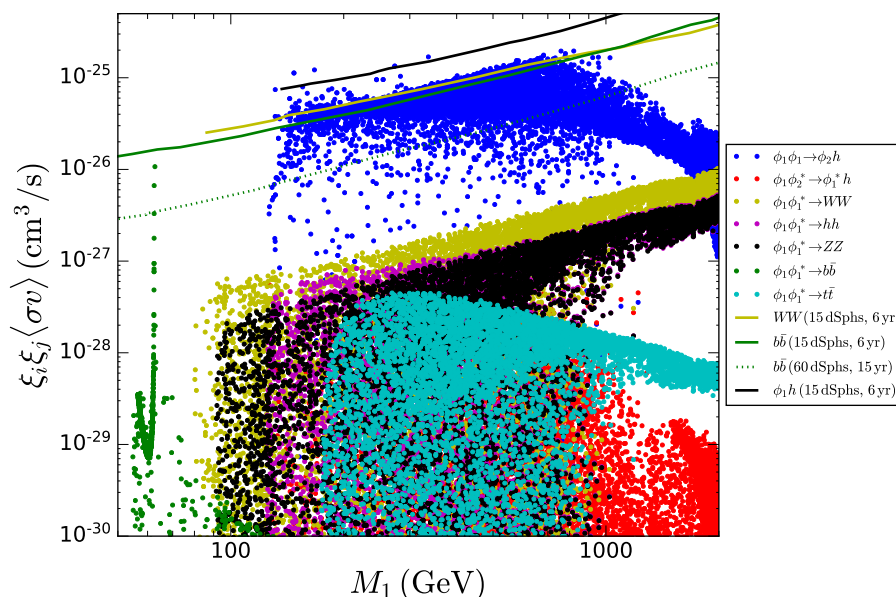
Figure 12. Dark matter annihilation rates for the viable models in the scan with $\mu_{S1} \neq 0$. The solid-green (solid-yellow) line shows current limit of ϕ_1 self-annihilation into $b\bar{b}$ (W^+W^-) reported by the Fermi collaboration from 6 years of observation and 15 dwarf spheroidal galaxies (dSphs) [28], while the dotted-green line represents the projected sensitivity for 45 dSphs and 15 years of observation [29] which serves as an estimate of the corresponding W^+W^- sensitivity since both bounds for 6 years as 15 dSphs are similar at high DM masses. Moreover, for comparison purposes the upper limit on the semi-annihilation process $\phi_1\phi_1^* \to \phi_1 h$ [36] is also displayed.

For ϕ_1, two regions can be clearly distinguished (see the left panel). If $M_1 \gtrsim 1\,\mathrm{TeV}$ — when the semi-annihilations are not as efficient — all viable points are at the brink of being detected, lying just below the current XENON1T limit. If $M_1 \lesssim 1\,\mathrm{TeV}$ instead, the (scaled) elastic scattering cross section varies over orders of magnitude, with some points close to the current limit and others located below the expected sensitivity of future experiments. For ϕ_2 (right panel), most of the detectable points feature $M_2 \lesssim 1.5\,\mathrm{TeV}$ while the non-detectable models are often characterized by a small value of $\xi_2 = \Omega_2/\Omega_{\mathrm{DM}}$. In this figure, the yellow points denote the viable models for which *both* dark matter particles are expected to yield signals in future direct detection experiments. If observed, such signals would rule out the *one dark matter particle paradigm* and open the way for multi-component dark matter scenarios such as the Z_5 model we are discussing.

With respect to indirect detection, the most relevant dark matter annihilation channels are displayed in figure 12 with their respective scaled cross sections. For comparison, the current limits [28] for certain final states are also shown (solid lines) as well as the projected sensitivity [29] for $b\bar{b}$ (dotted line). The semi-annihilation process $\phi_1 + \phi_1 \to \phi_2 + h$ turns out to be the most relevant one, with a cross section that can reach $10^{-25}\mathrm{cm}^3/\mathrm{s}$. The experimental limit on such a process will depend also on M_2 and has not been derived in the literature. A related process which has been considered is $\phi_1 + \phi_1 \to \phi_1 + h$, whose limit

is shown in the figure as a solid black line [36]. Since $M_2 > M_1$, the limit on $\phi_1 + \phi_1 \rightarrow \phi_2 + h$ should be weaker. Due to the ξ_2 suppression and its higher mass, the indirect detection signals involving ϕ_2 are less promising. Indirect detection experiments, therefore, do not constrain the viable parameter space of this model.

Let us summarize what we have found with the scan for $\mu_{S1} \neq 0$: i) the model becomes viable over the entire range of dark matter masses, $M_1 < 2$ TeV; ii) ϕ_1, the lighter dark matter particle, accounts for most of the dark matter density; iii) direct detection experiments offer great prospects to test this model, including the possibility of observing signals from *both* dark matter particles. As we wil see, ii) and iii) are actually generic features of the viable parameter space of the Z_5 model.

So far, we have examined the effect of μ_{S1} on the viable parameter space of the model, but what about the other couplings? Even if their effect on Ω_1 could not be observed in the examples given in the previous section, they may be present under certain circumstances. For that reason, we also did scans varying μ_{S2} and the dimensionless couplings.

The results for the scan with $\mu_{S2} \neq 0$ are shown in figure 13. In this case, we set the dimensionless couplings as well as μ_{S1} to zero ($\lambda_{3i}, \lambda_{412} = 0, \mu_{S1} = 0$) and vary μ_{S2} between 0.1 TeV and 10 TeV. Three crucial differences are observed with respect to the results from the μ_{S1} scan. First, there is a range of dark matter masses, above 1.1 TeV approximately, for which no viable models are found (top panels). Second, the dark matter masses have to be degenerate, with M_2/M_1 reaching a maximum value of about 1.3 for $M_1 \sim 100$ GeV and decreasing steeply with M_1 (top-left panel). Finally, it is the conversion process $\phi_1 + \phi_1 \rightarrow \phi_2 + \phi_2$ — mediated by a ϕ_2 — that reduces the ϕ_1 relic density over most of the viable range of M_1, with semi-annihilations being relevant only at low masses (top and center-left panels).

But there are also important similarities with the previous scan. The dark matter density is still dominated by the lighter component (ϕ_1) for all viable points (center-right panel), and direct detection experiments remain the most promising way to test this scenario in the near future (bottom panels). In particular, a significant fraction of models predict detectable signals from both dark matter particles (yellow points). Discriminating such signals would, however, become more challenging in this case due to the degeneracy between the dark matter particles.

In another scan we allowed the dimensionless couplings to independently vary within the range

$$0.1 \leq \lambda_{3i}, \lambda_{412} \leq 1. \tag{4.6}$$

while settting $\mu_{Si} = 0$. Semi-annihilations are absent in this case so the only new process that can reduce the ϕ_1 relic density is the conversion $\phi_1 + \phi_1 \rightarrow \phi_1 + \phi_2$, which is determined by λ_{31} and requires $M_1 \sim M_2$ not to be kinematically suppressed during freeze-out. The main results of this scan are displayed in figure 14. From the top-left panel we learn that there is a new viable region with $M_h/2 \lesssim M_1 \lesssim 400$ GeV that is characterized by a high degeneracy between the dark matter particles — M_2/M_1 never exceeds 1.1 there. As indicated by the value of ζ_{conv}^1, it is the above mentioned conversion process that renders such region consistent with current data. The top-right panel shows that ϕ_1
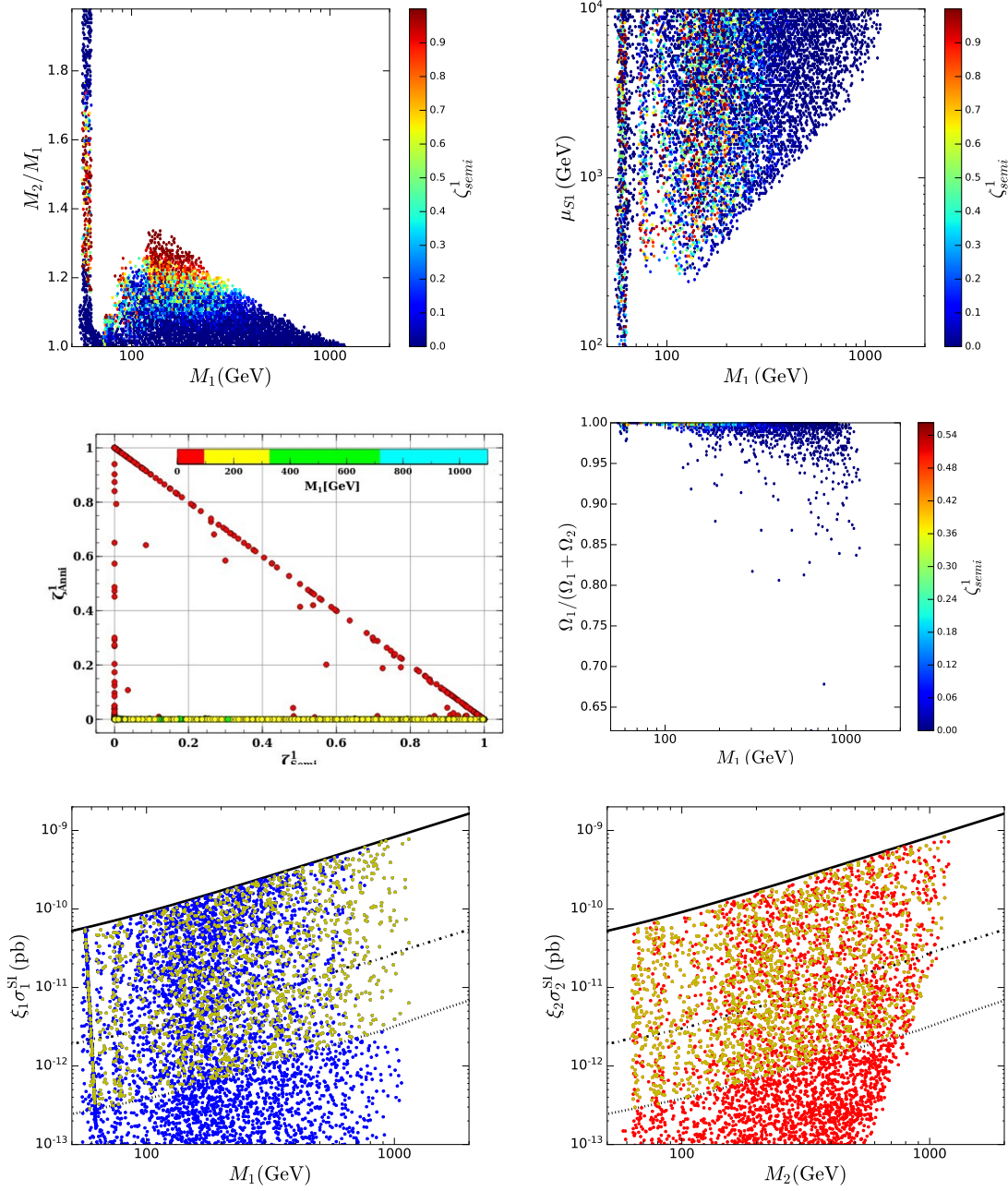
Figure 13. Results for the scan with $0.1 \leq \mu_{S2} \leq 10\,\mathrm{TeV}$, $\mu_{S1} = 0$ and $\lambda_{3i} = \lambda_{412} = 0$. Top panels: the viable parameter space; center panels: annihilation fraction vs semi-annihilation fraction and relative contribution of Ω_1 to Ω_{DM}; bottom panels: SI cross-sections scaled by ξ_i where the solid line is the upper limit set by XENON1T collaboration [25] and the dot-dashed (dotted) line is the projected sensitivity of LZ [26] (DARWIN [27]) experiment.

essentially accounts for the total dark matter density over the entire new viable region. The contribution of ϕ_2 amounts to less than 2%. In spite of this, either particle could be observed in future direct detection experiments, as illustrated in the bottom panels.
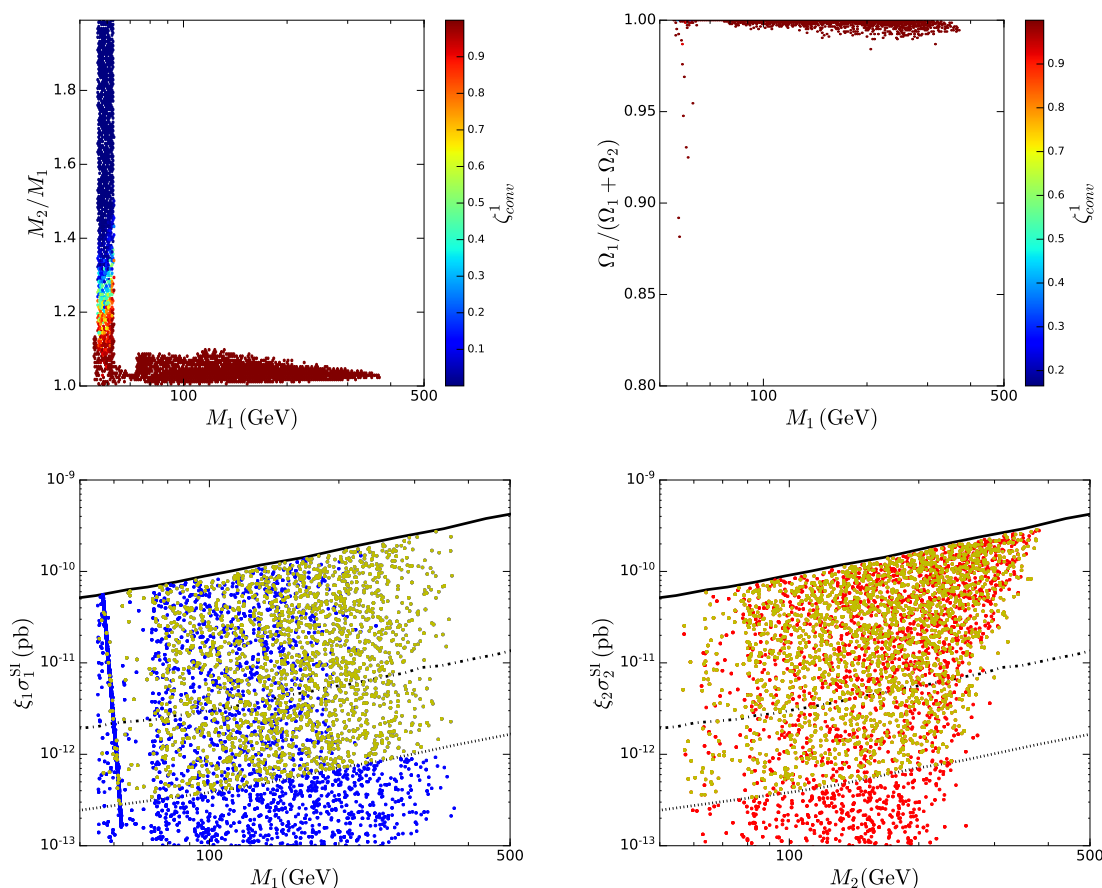
Figure 14. Scan results for $\mu_{Si} = 0$ with $\lambda_{3i} \neq 0$, $\lambda_{412} \neq 0$. Top panels: M_2/M_1 (left) and relative contribution of ϕ_1 to the total DM relic abundance (right) as a function of M_1. Bottom panels: spin-independent cross-sections for elastic scattering of ϕ_i with nuclei scaled by ξ_i. The solid line is the upper limit set by XENON1T collaboration [25] while the dot-dashed and dotted lines show the projected sensitivity of LZ [26] and DARWIN [27] experiments. Yellow points indicate that both DM particles lay within the sensitivity region of DARWIN.

We also did additional scans, including one in which *all* the free parameters of the model are simultaneously varied, and the results are essentially identical to what we found in the three scans already analyzed. It is fair to conclude, therefore, that our scans reveal the genuine viable parameter space of the Z_5 model.

In our analysis so far we have always assumed that $M_1 < M_2$ because, as already mentioned in section 2, the symmetry of the Lagrangian allows us to make this simplification. The results for the case $M_2 < M_1$ can be obtained from ours by simply swapping the corresponding quantities: $M_1 \leftrightarrow M_2$, $\mu_{S1} \leftrightarrow \mu_{S2}$, $\lambda_{31} \leftrightarrow \lambda_{32}$, $\Omega_1 \leftrightarrow \Omega_2$, etc. Thus, we have actually studied the full range of dark matter masses possible in this model — $M_1/2 < M_2 < 2M_1$.

In this section, the most important results of our work were derived — we characterized the viable parameter space of the Z_5 model and determined its detection prospects. Let

us review our main findings:

1. It is possible to satisfy the relic density constraint and current direct detection limits over the entire range of dark matter masses we considered ($M_1 < 2\,\mathrm{TeV}$). In particular, the low mass region $M \lesssim 1\,\mathrm{TeV}$, which is excluded in the singlet scalar model, is perfectly compatible with present bounds thanks to the new interactions allowed by the Z_5 symmetry.

2. The dark matter density is always dominated by the lighter dark matter particle. In our scans, the heavier dark matter particle never accounts for more than 40% of the total density, and often contributes significantly less than that.

3. Either dark matter particle may be detected in future direct detection experiments. And in a sizable fraction of models both particles are predicted to be detectable, providing a way to differentiate this model from the usual scenarios with just one dark matter particle.

Hence, besides being simple and well-motivated, the Z_5 model turns out to be a consistent and verifiable framework for two-component dark matter.

5 Discussion

We have seen that the new interactions allowed by the Z_5 symmetry render this model viable over a wide range of dark matter masses. This result stands in sharp contrast to what is found in similar models based on Z_2 symmetries. In the scenario with one complex scalar singlet stabilized by a Z_2 symmetry, the dark matter mass necessarily lies either at the Higgs-resonance or around $2\,\mathrm{TeV}$, as a consequence of the interplay between the relic density constraint and current direct detection limits. And a similar outcome is obtained in a two-dark matter scenario where the two singlet scalars are stabilized with a $Z_2 \times Z_2'$ symmetry. The Z_5 model can be seen as a natural extension of these scenarios and has the advantage of remaining viable at low masses and of being testable via direct detection experiments.

The Z_5 symmetry used in our model is the lowest Z_N compatible with two dark matter particles that are complex scalar fields[2] [12]. Even if other Z_N symmetries, with $N > 5$, can be imposed to simultaneously stabilize two dark matter particles [13], the Z_5 model serves as a prototype for *all* the two-component scenarios where the dark matter particles are complex scalars. That is, our results can be applied rather straightforwardly to other Z_N frameworks, as explained next.

Let us denote the two dark matter particles charged under a Z_N by ϕ_i, ϕ_j (with $i < j \leq N/2$ and $j \neq N/2$ for N even [12]), where ϕ_k gets a factor $e^{i2\pi k/N}$ upon a Z_N transformation. For $5 < N \leq 10$, the complete set of possibilities for the two dark matter particles is:

---

[2]Another interesting possibility is a Z_4 symmetry, which yields instead one complex and one real dark matter particle.

- (ϕ_1, ϕ_2): all Z_N symmetries allow the $\mu_{S1}\phi_1^2\phi_2^*$ term and forbid the $\mu_{S2}\phi_1\phi_2^2$ and $\lambda_{31}\phi_1^3\phi_2$ terms while the Z_7 is the only one that allows $\lambda_{32}\phi_1\phi_2^3$. This means that for the scenario with $M_1 < M_2$ the viable M_1 range can extend up to $2\,\mathrm{TeV}$ while for $M_2 < M_1$ the maximum value that M_2 can reach is $1\,\mathrm{TeV}$.

- (ϕ_1, ϕ_3): the Z_7 model allows $\mu_{S3}\phi_3^2\phi_1$ and $\lambda_{31}\phi_1^3\phi_3^*$ which implies a viable mass range up to $2\,\mathrm{TeV}$ ($1\,\mathrm{TeV}$) for $M_3 < M_1$ ($M_1 < M_3$). For Z_8 (Z_{10}), only the quartic interactions $\lambda_{31}\phi_1^3\phi_3^*$ and $\lambda_{33}\phi_3^3\phi_1^*$ ($\lambda_{31}\phi_1^3\phi_3^*$ and $\lambda_{33}\phi_3^3\phi_1$) are possible. Consequently, the viable mass range goes up to $400\,\mathrm{GeV}$ for both $M_1 < M_3$ and $M_3 < M_1$ cases. Since Z_9 only allows the term $\lambda_{31}\phi_1^3\phi_3^*$ a new viable mass range (up to $400\,\mathrm{GeV}$) is only recovered for $M_1 < M_3$.

- (ϕ_1, ϕ_4): Z_9 only allows the $\mu_{S4}\phi_4^2\phi_1$ term while Z_{10} forbids all the cubic (μ_{Si}) and quartic λ_{3i} interactions. Hence a new viable DM mass range is possible for Z_9 models.

- (ϕ_2, ϕ_3): the Z_7 model only has $\mu_{S2}\phi_2^2\phi_3$ and $\lambda_{33}\phi_3^3\phi_2^*$ interactions, which imply a viable mass range up to $2\,\mathrm{TeV}$ ($1\,\mathrm{TeV}$) for $M_2 < M_3$ ($M_3 < M_2$). In the Z_8 model only the $\mu_{S3}\phi_3^2\phi_2$ term is present such that the viable mass range goes up to $2\,\mathrm{TeV}$ ($1\,\mathrm{TeV}$) for $M_3 < M_2$ ($M_2 < M_3$). For Z_9 the trilinear interactions are forbidden and only the $\lambda_{32}\phi_2^3\phi_3$ term is allowed. Therefore a new viable mass range (up to $400\,\mathrm{GeV}$) is only recovered for $M_2 < M_3$. As in the previous item the Z_{10} model forbids both cubic (μ_{Si}) and quartic λ_{3i} interactions, which means there is no new viable DM regions.

- (ϕ_2, ϕ_4): the Z_9 only allows the $\mu_{S2}\phi_2^2\phi_4^*$ interaction, which implies a viable mass range up to $2\,\mathrm{TeV}$ ($1\,\mathrm{TeV}$) for $M_2 < M_4$ ($M_4 < M_2$). The case of the Z_{10} model is rather special since it features an analogous Lagrangian to the Z_5 model which means it allows both cubic (μ_{Si}) and quartic interactions λ_{3i}. Therefore the results presented in this work apply to the Z_{10} model with (ϕ_2, ϕ_4) as DM fields.

- (ϕ_3, ϕ_4): the Z_9 model only has the $\lambda_{34}\phi_4^3\phi_3^*$ interaction while the Z_{10} model only allows the $\mu_{S3}\phi_3^2\phi_4$ interaction. It follows that the viable DM mass range goes up to $2\,\mathrm{TeV}$ ($1\,\mathrm{TeV}$) for $M_3 < M_4$ ($M_4 < M_3$) in the Z_{10} model, while for Z_9 model a new viable mass range (up to $400\,\mathrm{GeV}$) is only recovered for $M_4 < M_3$.

This analysis demonstrates that the Z_5 model is the most general Z_N model with two complex fields, from which the DM properties for other models with a higher Z_N symmetry can be deduced to a large extent. By the same token, it is the Z_7 model with (ϕ_1, ϕ_2, ϕ_3) that serves as a prototype for scenarios with three dark matter particles.

Finally, let us comment on possible extensions of the Z_5 model. A simple one is to embed the Z_5 symmetry within an spontaneously broken U(1) gauge symmetry [12, 37]. In that case, the μ_{S1} term would still be allowed whereas the μ_{S2} would require an additional vacuum expectation value. Higher gauge symmetries can also be envisioned. Another option is to introduce extra fields so as to explain neutrino masses. By including additional vectorlike fermions, Majorana masses for the neutrinos can be generated at two-loops, as

in the Z_3-based models studied in [38–41]. The minimal extra fermion content turns out to be two $SU(2)_L$ doublets and one SM singlet, both having the same Z_5 charge (either w_5 or w_5^2) to admit a mixing term via the Higgs doublet. It follows that ϕ_1 and ϕ_2 become the loop mediators as in the scotogenic models and continue playing the role of DM particles as long as their decays into the new fermions are kinematically closed. Moreover, in certain regions of parameter space it may be possible to realize a scenario with 3 DM particles (two scalars plus a fermion) without additional symmetries. A phenomenological study of these interesting alternatives lies, however, beyond the scope of the present paper and will be left for future work.

6 Conclusions

We investigated the phenomenology of the two-component dark matter model based on a Z_5 symmetry, which serves as an archetype for other Z_N ($N > 5$) models with two complex scalar dark matter particles. After describing the model, we studied in detail how the relic density depends on the new parameters allowed by the Z_5 symmetry. In order to characterize the viable parameter space, we did several random scans and analyze their implications. We found that it is possible to satisfy the dark matter constraint and direct detection limits over the entire range of dark matter masses considered, $M_1 \lesssim 2\,\text{TeV}$. The key parameter turned out to be the trilinear coupling associated to the lighter dark matter particle (e.g. μ_{S1} for $M_1 < M_2$), which, via semi-annihilations, renders the model viable without requiring a mass degeneracy between the dark matter particles. At low dark matter masses ($M_i < 1\,\text{TeV}$), the other trilinear coupling as well as a quartic coupling (e.g. μ_{S2} and λ_{31} for $M_1 < M_2$) may also play a role, but only if the dark matter particles are at least mildly degenerate. We found that the dark matter density is dominated by the lighter particle for all the viable models and that a significant fraction of the viable parameter space can be probed by future direct detection experiments. Remarkably, *both* dark matter particles could give rise to observable signals in such experiments, providing a way not only to test this model but also to differentiate it from more conventional dark matter scenarios.

Acknowledgments

A Scalar potential constraints

General stability conditions are obtained from copositivity criteria [42, 43]. For $\lambda_{3i} = 0$ they read

$$\lambda_{4i} \geq 0, \ \ \Lambda_i \equiv \lambda_{Si} + 2\sqrt{\lambda_H \lambda_{4i}} \geq 0, \ \ \Lambda_3 \equiv \lambda_{412} + 2\sqrt{\lambda_{41}\lambda_{42}} \geq 0,$$
$$2\sqrt{\lambda_H \lambda_{41}\lambda_{42}} + \lambda_{S1}\sqrt{\lambda_{42}} + \lambda_{S2}\sqrt{\lambda_{41}} + \lambda_{412}\sqrt{\lambda_H} + \sqrt{\Lambda_1\Lambda_2\Lambda_3} \geq 0. \tag{A.1}$$

The corresponding expressions for $\lambda_{3i} \neq 0$ are rather involved and lengthy. However, taking into account that in our scans the free dimensionless parameters (their absolute values) are at most unity we highlight that the stability conditions may be fulfilled through not so large values for the self-interacting dark matter couplings λ_{4i}. On the other hand, the Z_5 symmetry is preserved by requiring that both ϕ_i do not acquire a vacuum expectation value.

B RGEs

The RGEs $dx/d(\ln\mu) = \beta_x^{(1)}/(16\pi^2)$ at one-loop level for the dimensionless scalar parameters are given by

$$\beta_{\lambda_{3i}}^{(1)} = 6\lambda_{3i}\Big(2\lambda_{4i} + \lambda_{412}\Big), \tag{B.1}$$

$$\beta_{\lambda_H}^{(1)} = \lambda_{S1}^2 + \lambda_{S2}^2 + \frac{27}{200}g_1^4 + \frac{9}{20}g_1^2g_2^2 + \frac{9}{8}g_2^4 - \frac{9}{5}g_1^2\lambda_H - 9g_2^2\lambda_H + 24\lambda_H^2 + 12\lambda_H y_t^2 - 6y_t^4, \tag{B.2}$$

$$\beta_{\lambda_{Si}}^{(1)} = \left[6y_t^2 - \frac{9}{10}g_1^2 - \frac{9}{2}g_2^2 + 12\lambda_H + 8\lambda_{4i}\right]\lambda_{Si} + 4\lambda_{Si}^2 + 2\lambda_{412}\lambda_{Sj}, \tag{B.3}$$

$$\beta_{\lambda_{4i}}^{(1)} = 20\lambda_{4i}^2 + 2\lambda_{Si}^2 + \frac{9}{2}|\lambda_{3i}|^2 + \lambda_{412}^2, \tag{B.4}$$

$$\beta_{\lambda_{412}}^{(1)} = 4\Big(2\lambda_{412}\lambda_{42} + 2\lambda_{41}\lambda_{412} + \lambda_{S1}\lambda_{S2} + \lambda_{412}^2\Big) + 9|\lambda_{31}|^2 + 9|\lambda_{32}|^2, \tag{B.5}$$

whilst for the dimensionful ones

$$\beta_{\mu_{S1}}^{(1)} = 4(\lambda_{412} + \lambda_{41})\mu_{S1} + 6\lambda_{31}\mu_{S2}^* + 6\lambda_{32}\mu_{S2}, \tag{B.6}$$

$$\beta_{\mu_{S2}}^{(1)} = 4(\lambda_{412} + \lambda_{42})\mu_{S2} + 6\lambda_{31}\mu_{S1}^* + 6\mu_{S1}\lambda_{32}^*, \tag{B.7}$$

$$\beta_{\mu_H^2}^{(1)} = 2\lambda_{S1}\mu_1^2 + 2\lambda_{S2}\mu_2^2 - \frac{9}{10}g_1^2\mu_H^2 - \frac{9}{2}g_2^2\mu_H^2 + 12\lambda\mu_H^2 + 6\mu_H^2 y_t^2, \tag{B.8}$$

$$\beta_{\mu_1^2}^{(1)} = 2\lambda_{412}\mu_2^2 + 2|\mu_{S1}|^2 + 4\lambda_{S1}\mu_H^2 + 8\lambda_{41}\mu_1^2 + |\mu_{S2}|^2, \tag{B.9}$$

$$\beta_{\mu_2^2}^{(1)} = 2\lambda_{412}\mu_1^2 + 2|\mu_{S2}|^2 + 4\lambda_{S2}\mu_H^2 + 8\lambda_{42}\mu_2^2 + |\mu_{S1}|^2. \tag{B.10}$$

These analytical expressions, which were derived by implementing the model in SARAH-4.12.3 [44, 45], were not used in our dark matter analysis but may be useful for other studies of the Z_5 model presented here.

Open Access. This article is distributed under the terms of the Creative Commons Attribution License ([CC-BY 4.0](#)), which permits any use, distribution and reproduction in any medium, provided the original author(s) and source are credited.

References

[1] C. Boehm, P. Fayet and J. Silk, *Light and heavy dark matter particles*, *Phys. Rev. D* **69** (2004) 101302 [hep-ph/0311143] [INSPIRE].

[2] E. Ma, *Supersymmetric Model of Radiative Seesaw Majorana Neutrino Masses*, *Annales Fond. Broglie* **31** (2006) 285 [hep-ph/0607142] [INSPIRE].

[3] Q.-H. Cao, E. Ma, J. Wudka and C.-P. Yuan, *Multipartite dark matter*, `arXiv:0711.3881` [ɪɴSPIRE].

[4] T. Hur, H.-S. Lee and S. Nasri, *A Supersymmetric* U(1)*-prime model with multiple dark matters*, *Phys. Rev. D* **77** (2008) 015008 [`arXiv:0710.2653`] [ɪɴSPIRE].

[5] H.-S. Lee, *Lightest U-parity Particle (LUP) dark matter*, *Phys. Lett. B* **663** (2008) 255 [`arXiv:0802.0506`] [ɪɴSPIRE].

[6] K.M. Zurek, *Multi-Component Dark Matter*, *Phys. Rev. D* **79** (2009) 115002 [`arXiv:0811.4429`] [ɪɴSPIRE].

[7] S. Profumo, K. Sigurdson and L. Ubaldi, *Can we discover multi-component WIMP dark matter?*, *JCAP* **12** (2009) 016 [`arXiv:0907.4374`] [ɪɴSPIRE].

[8] H. Baer, A. Lessa, S. Rajagopalan and W. Sreethawong, *Mixed axion/neutralino cold dark matter in supersymmetric models*, *JCAP* **06** (2011) 031 [`arXiv:1103.5413`] [ɪɴSPIRE].

[9] S. Esch, M. Klasen and C.E. Yaguna, *A minimal model for two-component dark matter*, *JHEP* **09** (2014) 108 [`arXiv:1406.0617`] [ɪɴSPIRE].

[10] B. Batell, *Dark Discrete Gauge Symmetries*, *Phys. Rev. D* **83** (2011) 035006 [`arXiv:1007.0045`] [ɪɴSPIRE].

[11] G. Bélanger, K. Kannike, A. Pukhov and M. Raidal, *Minimal semi-annihilating $\mathbb{Z}_N$ scalar dark matter*, *JCAP* **06** (2014) 021 [`arXiv:1403.4960`] [ɪɴSPIRE].

[12] C.E. Yaguna and Ó. Zapata, *Multi-component scalar dark matter from a Z_N symmetry: a systematic analysis*, *JHEP* **03** (2020) 109 [`arXiv:1911.05515`] [ɪɴSPIRE].

[13] G. Bélanger, F. Boudjema, A. Pukhov and A. Semenov, *MicrOMEGAs4.1: two dark matter candidates*, *Comput. Phys. Commun.* **192** (2015) 322 [`arXiv:1407.6129`] [ɪɴSPIRE].

[14] G. Arcadi, A. Djouadi and M. Raidal, *Dark Matter through the Higgs portal*, *Phys. Rept.* **842** (2020) 1 [`arXiv:1903.03616`] [ɪɴSPIRE].

[15] V. Silveira and A. Zee, *Scalar phantoms*, *Phys. Lett. B* **161** (1985) 136 [ɪɴSPIRE].

[16] J. McDonald, *Gauge singlet scalars as cold dark matter*, *Phys. Rev. D* **50** (1994) 3637 [`hep-ph/0702143`] [ɪɴSPIRE].

[17] C.P. Burgess, M. Pospelov and T. ter Veldhuis, *The Minimal model of nonbaryonic dark matter: A Singlet scalar*, *Nucl. Phys. B* **619** (2001) 709 [`hep-ph/0011335`] [ɪɴSPIRE].

[18] J.M. Cline, K. Kainulainen, P. Scott and C. Weniger, *Update on scalar singlet dark matter*, *Phys. Rev. D* **88** (2013) 055025 [*Erratum ibid.* **92** (2015) 039906] [`arXiv:1306.4710`] [ɪɴSPIRE].

[19] P. Athron, J.M. Cornell, F. Kahlhoefer, J. McKay, P. Scott and S. Wild, *Impact of vacuum stability, perturbativity and XENON1T on global fits of $\mathbb{Z}_2$ and $\mathbb{Z}_3$ scalar singlet dark matter*, *Eur. Phys. J. C* **78** (2018) 830 [`arXiv:1806.11281`] [ɪɴSPIRE].

[20] L.J. Hall, K. Jedamzik, J. March-Russell and S.M. West, *Freeze-In Production of FIMP Dark Matter*, *JHEP* **03** (2010) 080 [`arXiv:0911.1120`] [ɪɴSPIRE].

[21] C.E. Yaguna, *The Singlet Scalar as FIMP Dark Matter*, *JHEP* **08** (2011) 060 [`arXiv:1105.1654`] [ɪɴSPIRE].

[22] F. D'Eramo and J. Thaler, *Semi-annihilation of Dark Matter*, *JHEP* **06** (2010) 109 [`arXiv:1003.5912`] [ɪɴSPIRE].

[23] G. Bélanger, F. Boudjema, A. Pukhov and A. Semenov, *MicrOMEGAs_3: A program for calculating dark matter observables*, *Comput. Phys. Commun.* **185** (2014) 960 [arXiv:1305.0237] [INSPIRE].

[24] G. Bélanger, F. Boudjema, A. Goudelis, A. Pukhov and B. Zaldivar, *MicrOMEGAs5.0: Freeze-in*, *Comput. Phys. Commun.* **231** (2018) 173 [arXiv:1801.03509] [INSPIRE].

[25] XENON collaboration, *Dark Matter Search Results from a One Ton-Year Exposure of XENON1T*, *Phys. Rev. Lett.* **121** (2018) 111302 [arXiv:1805.12562] [INSPIRE].

[26] LUX-ZEPLIN collaboration, *Projected WIMP sensitivity of the LUX-ZEPLIN dark matter experiment*, *Phys. Rev. D* **101** (2020) 052002 [arXiv:1802.06039] [INSPIRE].

[27] DARWIN collaboration, *DARWIN: towards the ultimate dark matter detector*, *JCAP* **11** (2016) 017 [arXiv:1606.07001] [INSPIRE].

[28] FERMI-LAT collaboration, *Searching for Dark Matter Annihilation from Milky Way Dwarf Spheroidal Galaxies with Six Years of Fermi Large Area Telescope Data*, *Phys. Rev. Lett.* **115** (2015) 231301 [arXiv:1503.02641] [INSPIRE].

[29] FERMI-LAT collaboration, *Sensitivity Projections for Dark Matter Searches with the Fermi Large Area Telescope*, *Phys. Rept.* **636** (2016) 1 [arXiv:1605.02016] [INSPIRE].

[30] CMS collaboration, *Search for invisible decays of a Higgs boson produced through vector boson fusion in proton-proton collisions at $\sqrt{s} = 13\,TeV$*, *Phys. Lett. B* **793** (2019) 520 [arXiv:1809.05937] [INSPIRE].

[31] ATLAS collaboration, *Search for invisible Higgs boson decays with vector boson fusion signatures with the ATLAS detector using an integrated luminosity of $139\,fb^{-1}$*, ATLAS-CONF-2020-008 (2020).

[32] G. Bélanger, A. Mjallal and A. Pukhov, *Recasting direct detection limits within MicrOMEGAs and implication for non-standard Dark Matter scenarios*, arXiv:2003.08621 [INSPIRE].

[33] PLANCK collaboration, *Planck 2018 results. VI. Cosmological parameters*, arXiv:1807.06209 [INSPIRE].

[34] G. Duda, G. Gelmini and P. Gondolo, *Detection of a subdominant density component of cold dark matter*, *Phys. Lett. B* **529** (2002) 187 [hep-ph/0102200] [INSPIRE].

[35] G. Duda, G. Gelmini, P. Gondolo, J. Edsjo and J. Silk, *Indirect detection of a subdominant density component of cold dark matter*, *Phys. Rev. D* **67** (2003) 023505 [hep-ph/0209266] [INSPIRE].

[36] F.S. Queiroz and C. Siqueira, *Search for Semi-Annihilating Dark Matter with Fermi-LAT, H.E.S.S., Planck, and the Cherenkov Telescope Array*, *JCAP* **04** (2019) 048 [arXiv:1901.10494] [INSPIRE].

[37] S.-M. Choi and H.M. Lee, *Resonant SIMP dark matter*, *Phys. Lett. B* **758** (2016) 47 [arXiv:1601.03566] [INSPIRE].

[38] E. Ma, *Z(3) Dark Matter and Two-Loop Neutrino Mass*, *Phys. Lett. B* **662** (2008) 49 [arXiv:0708.3371] [INSPIRE].

[39] M. Aoki and T. Toma, *Impact of semi-annihilation of $\mathbb{Z}_3$ symmetric dark matter with radiative neutrino masses*, *JCAP* **09** (2014) 016 [arXiv:1405.5870] [INSPIRE].

[40] R. Ding, Z.-L. Han, Y. Liao and W.-P. Xie, *Radiative neutrino mass with* $\mathbb{Z}_3$ *dark matter: from relic density to LHC signatures*, *JHEP* **05** (2016) 030 [arXiv:1601.06355] [INSPIRE].

[41] S.-Y. Ho, T. Toma and K. Tsumura, *A Radiative Neutrino Mass Model with SIMP Dark Matter*, *JHEP* **07** (2017) 101 [arXiv:1705.00592] [INSPIRE].

[42] K. Kannike, *Vacuum Stability Conditions From Copositivity Criteria*, *Eur. Phys. J. C* **72** (2012) 2093 [arXiv:1205.3781] [INSPIRE].

[43] K. Kannike, *Vacuum Stability of a General Scalar Potential of a Few Fields*, *Eur. Phys. J. C* **76** (2016) 324 [*Erratum ibid.* **78** (2018) 355] [arXiv:1603.02680] [INSPIRE].

[44] F. Staub, *SARAH*, arXiv:0806.0538 [INSPIRE].

[45] F. Staub, *SARAH 4: A tool for (not only SUSY) model builders*, *Comput. Phys. Commun.* **185** (2014) 1773 [arXiv:1309.7223] [INSPIRE].